

The Role of r-Modes in Pulsar Spin-down, Pulsar Timing, and Gravitational Waves

Xiyuan Li^a, Shahram Abbassi^{a,*}, Varenva Upadhyaya^d, Xiyang Zhang^b, S. R. Valluri^{a,c}

^a*Department of Physics and Astronomy, University of Western Ontario, London, ON N6A 3K7, Canada*

^b*Department of Statistical and Actuarial Sciences, University of Western Ontario, London, ON N6A 3K7, Canada*

^c*Department of Mathematics, King's University College, University of Western Ontario, London, ON N6A 3K7, Canada*

^d*Department of Physics, Indian Institute of Technology, Hyderabad, Telangana 502284, India*

Abstract

We investigate the role of r-mode oscillations in pulsar spin-down and their implications for gravitational wave emission and pulsar timing analysis. Using a non-linear differential framework that includes r-mode contributions, we derive time-dependent solutions for rotational frequency and period evolution. These expressions are validated using observational data from the Crab pulsar with high precision. By analytically fitting braking indices and spin-down coefficients, we link measurable pulsar properties to gravitational wave signatures. Furthermore, we present closed-form expressions for neutron star compactness and tidal deformability using Lambert W and Lambert–Tsallis functions, enabling model-independent inferences from r-mode gravitational wave frequencies. Our results show that incorporating r-modes significantly improves the accuracy of spin-down models and continuous wave detectability, particularly through the inclusion of high-order frequency terms. This framework supports the modeling of timing residuals, glitch quantification, and gravitational wave constraints. Our findings have direct relevance for data analysis in ongoing and future gravitational wave observatories.

Keywords: pulsars, neutron stars, gravitational waves, r-modes, spin-down, timing, tidal deformability

1. Introduction

Neutron stars are among the most extreme astrophysical laboratories, hosting ultradense matter, strong magnetic fields, and rapid rotation. Pulsars—magnetized rotating neutron stars emitting periodic electromagnetic signals—lose angular momentum through various channels, including electromagnetic radiation, particle winds, and gravitational wave (GW) emission. The timing of pulsars, especially millisecond pulsars acting as highly stable cosmic clocks, provides powerful probes of these processes (1; 2; 3; 4).

A theoretically compelling mechanism for GW emission from rotating neutron stars involves the excitation of r-modes—toroidal, inertial oscillations restored by the Coriolis force and analogous to Rossby waves in terrestrial atmospheres (5; 6). These modes become unstable via the Chandrasekhar–Friedman–Schutz (CFS) mechanism when gravitational radiation drives the mode amplitude to grow faster than internal viscous dissipation can suppress it (7; 8; 9; 10). Once excited, r-modes can dominate angular momentum loss and significantly alter the spin evolution of young or rapidly rotating neutron stars.

The dissipation of r-modes is predicted to emit continuous, quasi-monochromatic gravitational waves, a key target for detectors such as LIGO, Virgo, and KAGRA

(11; 12). While the first detections (e.g., GW150914) involved compact binary mergers (11; 13), recent targeted searches have placed upper limits on r-mode amplitudes in individual pulsars such as PSR J0537–6910 (14). The r-mode instability has also been proposed as an explanation for the observed spin-down in the Crab pulsar (15; 16), and its evolution is known to be sensitive to factors such as crust elasticity, magnetic fields, differential rotation, and superfluidity (17; 18; 19; 20).

With next-generation detectors—Einstein Telescope (21), Cosmic Explorer (22), LISA (23), Taiji (24), and Tianqin (25)—the detection prospects for continuous waves from r-mode activity will improve significantly. Although low-frequency space-based detectors operate primarily in the nanohertz to millihertz range, they will inform high-frequency models by refining estimates of orbital dynamics and neutron star mass distributions. In parallel, Pulsar Timing Arrays (PTAs)—including NANOGrav, EPTA, PPTA, and the future Square Kilometer Array—offer complementary sensitivity to ultra-low-frequency GW signals by analyzing timing residuals across ensembles of millisecond pulsars (26; 27; 28; 29).

Despite these advances, several key questions remain unresolved. What is the precise impact of r-modes on observable spin-down behavior? Can gravitational wave signals from r-modes be detected within realistic sensitivities? And can such signals be used to constrain fundamental neutron star properties like the equation of state (EoS), compactness, and tidal deformability?

*Corresponding author

Email address: sabbassi@uwo.ca (Shahram Abbassi)

This work addresses these questions by developing a unified, analytical model that incorporates r-mode contributions to pulsar spin-down alongside electromagnetic and quadrupole GW torques. Using Lambert W and Lambert–Tsallis functions, we derive closed-form relationships connecting r-mode gravitational wave frequency to neutron star compactness and tidal deformability, generalizing previous approaches (16; 30). Our framework is EoS-independent, time-resolved, and applicable across the pre- and post-glitch evolution phases.

We validate our model using Crab pulsar data, demonstrating high-accuracy agreement in period evolution and braking indices. In particular, we show that including r-mode contributions improves spin-down modeling, enhances sensitivity to timing irregularities, and provides a pathway to constrain gravitational wave emission from isolated neutron stars.

The paper is structured as follows: Section 2 introduces the r-mode-augmented spin-down torque model. Section 3 develops analytical relations for rotational frequency, r-mode amplitude, compactness, tidal deformability, and pulsar period evolution. Section 4 focuses on period modeling and braking indices. Section 5 compares the model to observational data, with emphasis on glitch behavior and timing residuals. Section 6 discusses astrophysical implications, and Section 7 concludes. Detailed derivations are provided in Appendices Appendix B to Appendix D.

2. Spin-down Mechanisms

Pulsars lose rotational energy over time due to several dissipative mechanisms, with magnetic dipole radiation typically dominating the long-term spin evolution of isolated neutron stars (31; 32). However, for younger or faster-spinning pulsars, gravitational wave emission—especially through unstable oscillatory modes such as r-modes—can contribute significantly to the spin-down torque. This section analyzes how r-mode energy loss alters pulsar spin-down and connects with gravitational wave observables (33; 34; 35; 9).

Recent work has introduced simplified expressions for damping timescales associated with shear and bulk viscosity, both of which play critical roles in regulating r-mode growth and saturation (36; 37). The cumulative energy loss is inferred by considering the total change in rotational energy from all dominant channels (38):

$$\dot{E}_{\text{mono}} = -\beta \frac{\mu}{cR^2} \Omega^2, \quad (1)$$

$$\dot{E}_{\text{dip}} = -\frac{2\mu^2}{3c^3} \Omega^4, \quad (2)$$

$$\dot{E}_{\text{quad}} = -\frac{32GI^2e^2}{5c^5} \Omega^6, \quad (3)$$

$$\dot{E}_{\text{r-mode}} = -\frac{32\pi^2\alpha^2 JMR^3\Omega^8}{c^7}, \quad (4)$$

where $\Omega = 2\pi\nu$ is the angular frequency, μ is the magnetic dipole moment, R is the stellar radius, I the moment of inertia, e the ellipticity, and α the r-mode amplitude. J is a structural constant related to the stellar current quadrupole moment. The form of $\dot{E}_{\text{r-mode}}$ aligns with canonical derivations for unstable current-quadrupole r-mode dissipation (39; 15; 40).

For millisecond pulsars ($P < 1.5$ ms), variations in the moment of inertia may arise from internal structural changes, including phase transitions (41; 42). However, for slower rotators ($P \gtrsim 3$ ms), such variations are negligible and I can be treated as constant (38).

The spin frequency evolution can be connected to energy loss using:

$$E_{\text{rot}} = \frac{1}{2} I \Omega^2, \quad (5)$$

$$\dot{\nu} = \frac{1}{4\pi^2 I} \cdot \frac{\dot{E}_{\text{rot}}}{\nu}.$$

Equation (5) forms the basis for modeling multi-channel torque effects. A generic spin-down model takes the form:

$$\dot{\nu} = k\nu^n, \quad (6)$$

where k is a constant and n is the braking index, which reflects the dominant energy loss process. To capture additional physical processes, including gravitational wave emission and r-mode losses, we generalize the model as:

$$\dot{\nu} = -s(t)\nu - r(t)\nu^3 - g(t)\nu^5 - l(t)\nu^7, \quad (7)$$

where s , r , g , and l represent frequency-dependent coefficients corresponding to monopole, dipole, quadrupole, and r-mode current-quadrupole losses, respectively.

Each term in Eq. (7) corresponds to a specific physical mechanism: magnetic monopole (ν^1), dipole radiation (ν^3), quadrupole deformation (ν^5), and r-mode emission (ν^7), which maps to an $n = 8$ braking index. Such a steep frequency dependence is characteristic of current-quadrupole gravitational radiation. The effect of these terms becomes pronounced in young, hot neutron stars or those with substantial internal fluid motion (15; 40).

In addition to axisymmetric deformations, high-order multipoles such as octupoles or baroclinic modes may be present in certain exotic systems, although these are not included in our model (43; 44).

Ultimately, r-mode-driven gravitational radiation growth is governed by the CFS mechanism (45; 46). When r-mode growth timescales are shorter than viscous damping, the mode becomes unstable, causing a strong angular momentum outflow via gravitational waves. This process introduces a measurable spin-down signal. Numerous works have modeled the associated frequencies and detection strategies (39; 47; 40; 30; 48; 49; 50).

In the next section, we incorporate these mechanisms into analytical and numerical models to study compactness, deformability, r-mode amplitudes, and spin-down behavior.

3. r-mode Formalism and Analytical Solutions

3.1. Rotational and Gravitational Wave Frequencies from *r*-modes

The r-mode oscillation frequency ω in a rotating neutron star is governed by its angular frequency Ω and the mode's angular indices l and m , given by:

$$\omega = -m\Omega + \frac{2m\Omega}{l(l+1)}, \quad (8)$$

where l and m specify the spherical harmonic degree and azimuthal order, respectively (6; 51). We consider the fundamental $l = m = 2$ r-mode, which dominates gravitational radiation among inertial modes (52; 53; 54). This analysis assumes barotropic stellar structure, neglecting buoyancy effects associated with the Brunt–Väisälä frequency. While this enables analytical tractability, future studies may incorporate stratification for a more realistic model of neutron star interiors.

For $l = m$, the r-mode angular frequency simplifies to:

$$\omega = -\frac{(l+2)(l-1)}{l+1}\Omega, \quad (9)$$

and the corresponding gravitational wave frequency is:

$$f_{gw} = -\frac{2}{3\pi}\Omega. \quad (10)$$

Equation (10) is valid in the Newtonian regime. However, neutron stars are compact and rapidly rotating, necessitating general relativistic (GR) corrections. For this, we adopt a higher-order approximation (55; 30):

$$f_{gw} = A\nu - \frac{B}{\nu_k^2}\nu^3, \quad (11)$$

where ν is the spin frequency (Hz), ν_k is the Keplerian breakup frequency, the upper spin limit for stable pulsar rotation that can be determined analytically (56; 15). A typical ν_k for a neutron star on the lower-end of the mass range is 506 Hz (55). The parameters A and B encapsulate GR and rotational corrections, respectively:

$$\begin{aligned} 1.39 \leq A \leq 1.57, \\ 0 \leq B \leq 0.195. \end{aligned} \quad (12)$$

Values of A reflect frame dragging and spacetime curvature in slowly rotating stars, while B accounts for centrifugal flattening and nonlinear rotational effects (54; 55; 49).

Equation (11) is non-linear in ν , making analytical inversion difficult. We resolve this by applying the Lambert–Tsallis function, a generalization of the Lambert W function suitable for non-linear systems. The q -exponential used in the Tsallis formalism is defined as:

$$\exp_q z = [1 + (1-q)z]^{\frac{1}{1-q}}, \quad q \neq 1. \quad (13)$$

The Lambert–Tsallis function $W_q(z)$ satisfies:

$$W_q(z) \exp_q W_q(z) = z, \quad z \in \mathbb{R}. \quad (14)$$

Solving Eq. (11) with this approach yields:

$$\nu_1 = \left[-\frac{A}{2B}\nu_k^2 W_{1/2} \left\{ -\frac{2B}{A\nu_k^2} \left(\frac{f_{gw}}{A} \right)^2 \right\} \right]^{1/2}, \quad (15)$$

$$\nu_2 = \left[\frac{3B}{2A\nu_k^2} W_{5/2} \left\{ \frac{2A\nu_k^2}{3B} \left(\frac{-f_{gw}\nu_k^2}{B} \right)^{-2/3} \right\} \right]^{-1/2}. \quad (16)$$

These solutions offer a path to estimate ν from f_{gw} analytically, bypassing numerical inversion. For PSR J0537–6910, a young pulsar with $\nu = 62$ Hz (57), inserting A and B into Eq. (11) gives an r-mode GW frequency of 86–98 Hz—well within LIGO's sensitivity band (14; 30). From Eq. (15), we find the rotational frequency range $62.00 \leq \nu_1 \leq 62.42$ Hz, consistent with expected values. However, ν_2 from Eq. (16) lies outside physical bounds and is excluded.

This analytic method provides an elegant way to probe the spin evolution of neutron stars via gravitational wave frequency measurements and can be extended to study braking indices and timing residuals.

3.2. Structural Inference: Compactness and Tidal Deformability from *r*-modes

The compactness of a neutron star, defined as $C = M/R$, influences its r-mode gravitational wave frequency. A phenomenological model that captures this relationship is given by:

$$f_r = a_1 \left(\frac{M}{R} \right) - a_2 \left(\frac{M}{R} \right)^2 + a_3, \quad (17)$$

where a_1 , a_2 , and a_3 are empirical coefficients fitted using tabulated EoS models (48; 30). This quadratic form provides an intuitive interpolation between r-mode frequency and compactness.

By approximating Eq. (17) in the limit of small C , we obtain:

$$f_r - a_3 = -a_2 C^2 \exp \left\{ -\frac{a_1}{a_2} \cdot \frac{1}{C} \right\}, \quad (18)$$

which can be analytically inverted using the Lambert W function to yield:

$$C = \frac{a_1}{2a_2} \left(W \left\{ \frac{a_1}{2a_2} \sqrt{\frac{a_2}{a_3 - f_r}} \right\} \right)^{-1}, \quad (19)$$

where $W(z)$ is the Lambert W function satisfying $W(z) \exp\{W(z)\} = z$ (58).

Although Eq. (17) appears independent of spin frequency, the compactness and tidal deformability implicitly contain rotational information via their dependence on stellar structure. As shown in (30), the r-mode frequency encapsulates rotational and structural dynamics, enabling these quantities to be inferred from GW observations.

In Figure 1, we fit Eq. (19) to data from 14 tabulated EoSs (48). The best-fit parameters— $a_1 = -0.184$, $a_2 = 1.640$, $a_3 = 0.667$ —yield $R^2 = 0.9972$, confirming the

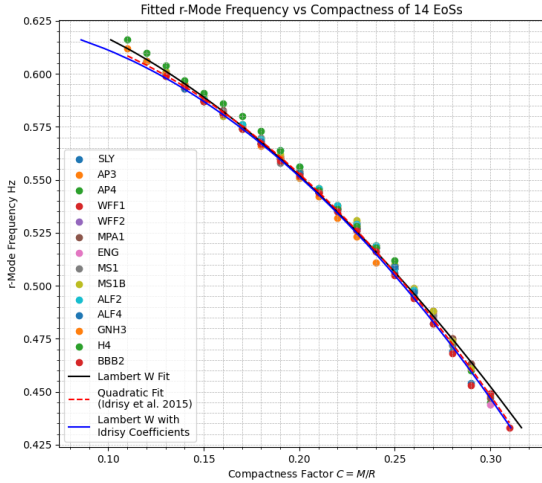


Figure 1: Fitted r-mode gravitational wave frequency versus compactness $C = M/R$ for 14 tabulated equations of state (EoSs) (48). Solid black line: Lambert W solution given by Eq. (19), with best-fit coefficients $a_1 = -0.184$, $a_2 = 1.640$, and $a_3 = 0.667$, achieving an R^2 value of 0.9972. Dashed red line: Quadratic model, with best-fit coefficients $a_1 = 0.079$, $a_2 = 2.25$, and $a_3 = 0.627$ from Idrisy et al. 2015 (48). Solid blue line: Lambert W solution with Idrisy quadratic model coefficients.

The Lambert W fit provides a superior match to the numerical data, capturing the nonlinear dependence of r-mode frequency on compactness across a wide range of realistic neutron star models.

robustness of the Lambert W solution. We also evaluated the frequency estimation performance of the quadratic model and the Lambert W model using the same set of best-fit coefficients from Idrisy et al. 2015 (48). The maximum difference between the two estimated frequencies is within 0.34%. Equation 19 provides a closed-form expression for estimating neutron star compactness from r-mode GW frequency, independent of the EoS.

Tidal deformability Λ characterizes a star's response to tidal perturbations and also affects r-mode evolution. It is defined as:

$$\Lambda = \frac{2}{3}k_2 \left(\frac{R}{M} \right)^5, \quad (20)$$

where k_2 is the dimensionless Love number (59; 60). The r-mode frequency is indirectly influenced by Λ through changes in the star's density distribution and moment of inertia.

A quadratic model relating f_r to $\ln \Lambda$ is:

$$f_r = b_1 \ln \Lambda + b_2 (\ln \Lambda)^2 + b_3, \quad (21)$$

where b_1 , b_2 , b_3 are fitted coefficients (61). Under the assumption that $b_2 < 0$ (61; 30), and $\frac{-b_2}{b_1} \ln \Lambda \ll 1$, Eq. (21) becomes:

$$\frac{b_2}{b_1^2}(f_r - b_3) = \frac{b_2}{b_1} \ln \Lambda \cdot \exp \left\{ \frac{b_2}{b_1} \ln \Lambda \right\}, \quad (22)$$

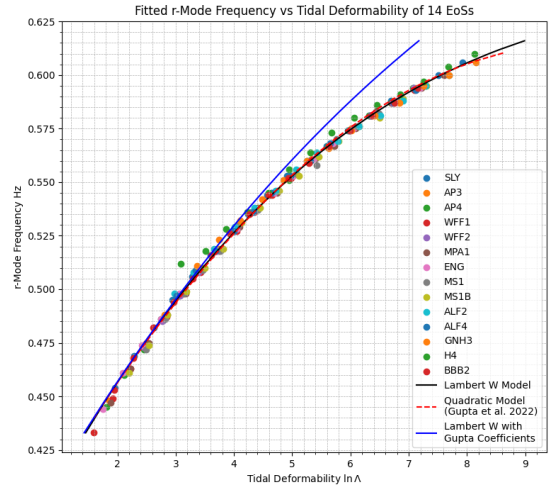


Figure 2: Fitted r-mode gravitational wave frequency as a function of tidal deformability $\ln \Lambda$ for 14 tabulated EoSs (48), computed using LALSuite (62). Solid black line: Lambert W fit (Eq. (23)) with best-fit coefficients $b_1 = 0.0568$, $b_2 = -0.0043$, and $b_3 = 0.3591$, achieving an R^2 value of 0.998. Dashed red line: Quadratic model, with best-fit coefficients $b_1 = 0.0498$, $b_2 = -0.0025$, and $b_3 = 0.3668$ from Gupta et al. 2022 (61). Solid blue line: Lambert W solution with Gupta quadratic model coefficients.

The Lambert W model provides a highly accurate, analytical, EoS-independent mapping between tidal deformability and r-mode frequency.

which has an analytical solution via the Lambert W function:

$$\ln \Lambda = \frac{b_1}{b_2} W \left\{ \frac{b_2}{b_1^2} (f_r - b_3) \right\}. \quad (23)$$

Figure 2 shows the fit of Eq. (23) to data obtained using the TOV solver in LALSuite (62). Compactness inputs are taken from (48). Although ν does not appear explicitly, its influence is implicit through compactness and structural changes. The best-fit values— $b_1 = 0.0568$, $b_2 = 0.0043$, $b_3 = 0.3591$ —achieve $R^2 = 0.998$, demonstrating excellent agreement. When our Lambert W model and the Gupta-like quadratic model were evaluated using the same set of best-fit coefficients from Gupta et al. 2022 (61), the maximum difference between the two estimated frequencies is within 3.25%.

3.3. Time-Dependent Amplitude and Energy Loss

The evolution of r-mode amplitude α and stellar spin Ω in a rotating neutron star can be modeled as a coupled two-variable system. Following the formalism of (63), we begin with:

$$\frac{d\alpha}{dt} = -\frac{\alpha}{\tau_{GR}} - \frac{\alpha}{\tau_V} \cdot \frac{1 - \alpha^2 Q}{1 + \alpha^2 Q}, \quad (24)$$

$$\frac{d\Omega}{dt} = -\frac{2\Omega}{\tau_V} \cdot \frac{\alpha^2 Q}{1 + \alpha^2 Q}, \quad (25)$$

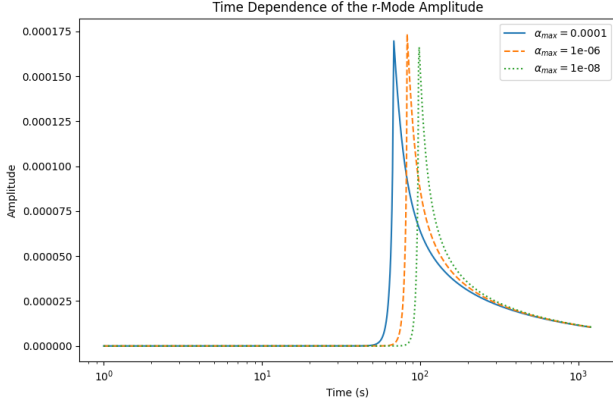


Figure 3: Time dependence of the r-mode amplitude α . The amplitude grows into the saturation mode near $t = 10^2$ s, where the non-linear effects can no longer be ignored. The r-mode amplitude settles to a gradual decay that dominates the rest of the time.

Here, $Q = 3\tilde{J}/2\tilde{I}$ is a dimensionless structural parameter dependent on the equation of state. \tilde{J} and \tilde{I} are normalized stellar structure coefficients, while τ_{GR} and τ_V are the gravitational radiation and viscous damping timescales, respectively (39).

Equation (24) can be rewritten in a more tractable form:

$$\frac{\tau_{GR}\tau_V(1 + \alpha^2 Q) d\alpha}{\alpha[(\tau_V + \tau_{GR}) + \alpha^2(\tau_V Q - \tau_{GR} Q)]} = -dt, \quad (26)$$

Defining:

$$\xi_1 = \tau_{GR}\tau_V, \quad T_A = \tau_{GR} + \tau_V, \quad T_B = Q(\tau_V - \tau_{GR}),$$

we simplify Eq. (26) as:

$$\frac{\xi_1(1 + \alpha^2 Q) d\alpha}{\alpha(T_A + \alpha^2 T_B)} = -dt. \quad (27)$$

Upon integrating and inverting the expression using the Lambert W function, the amplitude α becomes:

$$\alpha(t) = \left(\frac{1}{2\xi_c} W \left[2\xi_c \exp \left(-\frac{2(t + \xi_B \ln T_A - c_1)}{\xi_A} \right) \right] \right)^{1/2}, \quad (28)$$

where the intermediate coefficients are:

$$\begin{aligned} \xi_A &= \xi_1/T_A, \\ \xi_B &= \frac{Q\xi_1}{2T_B} - \frac{\xi_1}{2T_A}, \\ \xi_c &= \frac{T_B\xi_B}{T_A\xi_A}. \end{aligned}$$

The corresponding spin frequency is given by $\nu = \Omega/(2\pi)$, which varies with time according to Eq. (25).

To connect with observations, we relate the r-mode amplitude α to the gravitational wave strain h_0 via (49):

$$\alpha = \left(\frac{5}{8\pi} \right)^{1/2} \frac{c^5}{G} \cdot \frac{h_0}{(2\pi f_{gw})^3} \cdot \frac{d}{MR^3\tilde{J}}, \quad (29)$$

where f_{gw} is the gravitational wave frequency, d is the source distance, M and R are the mass and radius of the neutron star, and \tilde{J} reflects the current quadrupole normalization.

These expressions link the r-mode amplitude and its evolution to gravitational wave observables. The inclusion of the Lambert W function enables analytical tracking of $\alpha(t)$ across viscous and radiative timescales, offering a predictive framework for gravitational wave data analysis in the context of r-mode-driven signals.

Furthermore, our amplitude formulation is consistent with observational upper limits reported by (16), who found that r-mode amplitudes in sources such as the Crab pulsar are likely bounded by $\alpha \lesssim 10^{-4}$. These empirical constraints provide essential context for interpreting Eq. (29), particularly in relation to gravitational wave detectability using current and future detectors.

4. Pulsar Period Modeling and Spin-down Coefficients

4.1. Period Evolution with Time-Dependent Spin-down Parameters

We extend our spin-down model by deriving a closed-form expression for the time evolution of the pulsar period $P(t)$, following the non-linear formalism of (64). The model applies to isolated pulsars and incorporates time-dependent spin-down coefficients $\{s(t), r(t), g(t), l(t)\}$, as introduced in Eq. (7).

The model's consistency is validated against observed frequency derivatives and braking indices from (65), and with data from the ATNF Pulsar Database. For the Crab pulsar, our predicted periods match observed values with a relative error of 0.02%, as shown in Table 3.

Rewriting Eq. (7) in terms of the period $P = 1/f$, where f is the pulsar frequency, and factoring out P^5 , yields:

$$P^5 \frac{dP}{dt} = (s_0 P^6 + r_0 P^4 + g_0 P^2 + l_0) \left(1 + \frac{t}{t_c} \right)^{-2}, \quad (30)$$

where t_c is the magnetic field decay timescale. Defining $K = P^2$ and using $dK = 2PdP$, Eq. (30) becomes:

$$\frac{K^2 dK}{2s_0[(K-a)(K-b)(K-c)]} = \left(1 + \frac{t}{t_c} \right)^{-2} dt, \quad (31)$$

where a, b, c are the roots of the spin-down polynomial. Integrating Eq. (31) yields:

$$\begin{aligned} & 2[(x-a)(x^2-y^2)+2xy^2] \tan^{-1} \left(\frac{y(K_0-K)}{(K-x)(K_0-x)+y^2} \right) + \\ & [y(x^2-y^2)-2xy(x-a)] \ln \left(\frac{(K-x)^2+y^2}{(K_0-x)^2+y^2} \right) \\ & - 2ya^2 \ln \left(\frac{K-a}{K_0-a} \right) = -4ys_0t(x^2-2ax+a^2+y^2), \end{aligned} \quad (32)$$

Function	Value (Crab PSR B0531+21)
$\ln \left[\frac{(K-x)^2 + y^2}{(K_0-x)^2 + y^2} \right]$	0.0158
$\tan^{-1} \left[\frac{y(K_0-K)}{(K-x)(K_0-x) + y^2} \right]$	-0.066
$\ln \left[\frac{K-a}{K_0-a} \right]$	0.0540

Table 1: Approximate values for logarithmic and arctangent terms in Eq. (32) for the Crab pulsar, enabling Taylor expansion.

where x and y are defined through the complex root structure of the cubic. Table 1 provides term-by-term estimates for the Crab pulsar.

Using Taylor expansion for small deviations, Eq. (32) simplifies to:

$$\begin{aligned}
(K-K_0) \left[\frac{\lambda_3}{(K-x)(K_0-x) + y^2} + \lambda_1(K+K_0-2x) + \lambda_2 \right] \\
= -\lambda_s t, \\
\text{where } \lambda_1 = \frac{2ax - x^2 - y^2}{(q_0 - x)^2 + y^2}, \\
\lambda_2 = \frac{-2a^2}{K_0 - a}, \quad \lambda_3 = 2(x^3 - ax^2 + ay^2 + xy^2), \\
\lambda_s = 4s_0((x-a)^2 + y^2). \quad (33)
\end{aligned}$$

Table 2 summarizes λ terms for various pulsars. λ_1 is typically small and may be neglected.

Eq. (33) leads to a quadratic equation in K :

$$\begin{aligned}
\alpha_1 K^2 + (\alpha_2 + \lambda_a t)K + \alpha_3 + \lambda_b t &= 0, \\
\text{with } \alpha_1 &= \lambda_2(K_0 - x), \\
\alpha_2 &= \lambda_3 + \lambda_2(x^2 - y^2 - K_0^2), \\
\alpha_3 &= K_0[\lambda_2(K_0 x - x^2 + y^2) - \lambda_3], \\
\lambda_a &= -\lambda_s(K_0 - x), \quad \lambda_b = -\lambda_s(K_0 x - x^2 + y^2). \quad (34)
\end{aligned}$$

Solving the quadratic yields a time-dependent period:

$$P(t) = \sqrt{\frac{1}{2\alpha_1} \left\{ -\alpha_2 - \lambda_a t + \sqrt{(\alpha_2 + \lambda_a t)^2 - 4\alpha_1(\alpha_3 + \lambda_b t)} \right\}}. \quad (35)$$

Table 3 presents parameter values for the Crab pulsar, showing excellent agreement with observed values.

For Eq. (35) to yield real values, the discriminant must be positive, imposing the condition:

$$t^2 \leq \frac{(2\lambda_a \alpha_2 - 4\alpha_1 \lambda_b)^2}{4\lambda_a^2(\alpha_2^2 - 4\alpha_1 \alpha_3)}. \quad (36)$$

Thus, Eq. (35) provides a compact expression for pulsar period evolution in terms of initial conditions and spin-down coefficients. It can be used to extract age and spin-down histories in conjunction with observational timing data.

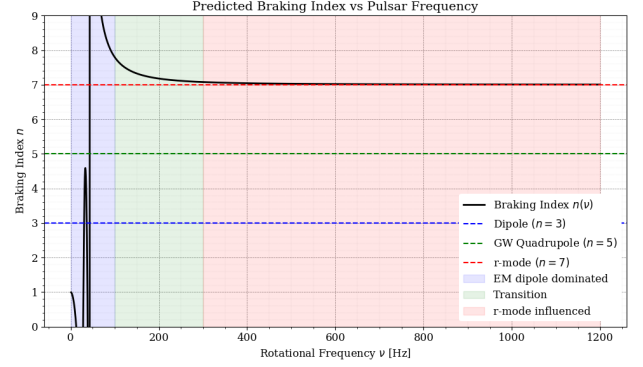


Figure 4: Braking index n as a function of rotational frequency ν for a model including electromagnetic, gravitational wave, and r-mode contributions. At low frequencies, the braking index approaches $n \approx 3$, consistent with magnetic dipole spin-down. As the spin increases, the gravitational wave terms dominate, especially the ν^7 r-mode component, causing n to asymptotically rise toward $n \approx 7-8$. This curve reflects Eq. (40) with representative coefficients from Table 5.

4.2. Braking Indices

The braking index n characterizes the deviation from a uniform spin-down and offers insight into the torque mechanisms acting on neutron stars. Equation (6) relates the spin-down rate to a power-law in rotational frequency:

$$\dot{\nu} = -k\nu^n, \quad (37)$$

where k is a constant and n is the braking index. In the classical case of magnetic dipole radiation, $n = 3$ (66).

Different braking indices reflect different dominant energy-loss mechanisms: $n = 1$ for particle winds, $n = 5$ for gravitational wave emission due to a mass quadrupole, and $n = 7-8$ for current-quadrupole radiation such as r-modes.

Braking indices can also be defined observationally using derivatives of the spin frequency:

$$n = \frac{\ddot{\nu}\nu}{\dot{\nu}^2}, \quad (38)$$

$$m = \frac{\ddot{\nu}\nu^2}{\dot{\nu}^3}, \quad (39)$$

where m is the second braking index. These indices capture deviations in the timing residuals and track evolving spin-down behavior.

R-mode instabilities are known to modify spin-down behavior through enhanced gravitational radiation. Previous studies (36; 67) showed that the instability window is shaped by viscous damping: bulk viscosity dominates at high temperatures ($\tau_{\text{bulk}} \propto \Omega^{-2}$), while shear viscosity controls the low-temperature regime ($\tau_{\text{shear}} \propto \Omega^{-1}$).

Using the spin-down formulation of Eq. (7), the braking indices can be expressed analytically as:

$$n = \frac{s + 3r\nu^2 + 5g\nu^4 + 7l\nu^6}{s + r\nu^2 + g\nu^4 + l\nu^6}, \quad (40)$$

PSR	$\lambda_1(K + K_0 - 2x)$	λ_2	$\lambda_3/((K - x)(K_0 - x) - y^2)$	λ_s
J0007+7303	0.012	-0.60	6160.00	2.167×10^{-7}
B0531+21 (Crab)	-4.815×10^{-7}	-9.586×10^{-4}	-8.638×10^{-3}	5.589×10^{-9}
J1023-5746	0.00028	-0.52	-43.37	5.71×10^{-9}
J1418-6058	0.00025	-0.23	-650.16	1.10×10^{-8}

Table 2: Fitted λ terms for four representative pulsars from the ATNF database.

PSR	Parameter/Variable	Value
Crab PSR B0531+21	α_1	-3.967×10^{-8}
	α_2	2.284×10^{-9}
	α_3	-2.489×10^{-12}
	λ_a	1.104×10^{-20}
	λ_b	-7.376×10^{-23}
	P_0	33.333 ms
	P (calculated)	33.808 ms
	P (observed)	33.814 ms

Table 3: Parameter values in Eq. (35) for the Crab pulsar, based on Jodrell Bank ephemerides between MJD 46812 and 60050. Relative error: 0.02%.

$$m = \frac{s + 3r\nu^2 + 5g\nu^4 + 7l\nu^6}{s + r\nu^2 + g\nu^4 + l\nu^6} + 2\nu^2 \cdot \frac{3r + 10g\nu^2 + 21l\nu^4}{s + r\nu^2 + g\nu^4 + l\nu^6}. \quad (41)$$

We evaluate these expressions for selected pulsars using the spin-down parameters in Table 5. The results are compared to observed values in Table 4, showing excellent agreement in most cases. Larger deviations in high-braking pulsars may be due to timing noise or glitches.

Figure 4 complements Table 4 by illustrating the theoretical behavior of the braking index n as a function of rotational frequency ν . The figure reveals a clear transition: at low frequencies ($\nu \lesssim 10$ Hz), the braking index converges toward the magnetic dipole value $n \approx 3$, while at higher frequencies, the influence of r-mode emission becomes dominant, driving $n \rightarrow 7-8$. This behavior aligns with the hierarchy of spin-down contributions modeled in Eq. (7), where the ν^7 term due to r-mode energy loss increasingly dominates. The figure provides a visual diagnostic for interpreting pulsar braking indices and identifying whether gravitational or electromagnetic mechanisms govern their spin evolution.

These expressions demonstrate how r-mode contributions and spin-down coefficients influence pulsar evolution, and provide theoretical support for observed braking behavior in both young and middle-aged neutron stars. The additional frequency-dependent plot further reveals how braking index trends can distinguish between energy-loss mechanisms across rotational regimes.

5. Period Analysis with Glitching Crab Pulsar PSR B0531+21 Data

To validate our period model, we apply it to the well-studied Crab pulsar (PSR B0531+21), using timing data spanning several decades. This section also includes comparisons to other pulsars for generality.

We use monthly ephemeris data (in CGRO format) from Jodrell Bank Observatory (70), expressed in Barycentric Dynamic Time (TDB). The dataset spans from January 1987 to September 2023. Glitch times are extracted from the glitch notes provided by the observatory, including the most recent major glitch in November 2017. Glitches are treated as breakpoints for fitting purposes.

The pulsar frequency is modeled using a Taylor expansion:

$$f(t) = f_0 + f'_0(t - t_0) + \frac{1}{2}f''_0(t - t_0)^2 + \frac{1}{6}f'''_0(t - t_0)^3 + \frac{1}{24}f''''_0(t - t_0)^4 + \delta f(t), \quad (42)$$

Observed frequencies and derivatives are evaluated between glitches as listed in Table 6, using MJD 47084 as the reference point.

Figure 5 compares observational data with two fitting strategies: one continuous fit over the entire dataset and separate fits between individual glitches. Between-glitch fits yield a mean deviation of $P(t) - P_{\text{obs}} = -1.166 \times 10^{-7}$, while the long-term fit shows a larger average deviation of -6.105×10^{-5} . Discrepancies between models and observations highlight glitch-induced irregularities, particularly visible in the zoomed-in region (MJD 53250 to 54000).

Figure 6 plots the relative error for both fitting strategies. The long-term fit shows a systematic exponential drift, while short-term fits exhibit sharp changes near known glitch epochs.

Incorporating r-mode effects: Post-glitch recovery and longer-term spin-down evolution may be modulated by r-mode oscillations, which influence angular momentum redistribution. These modes could be responsible for part of the gradual post-glitch convergence.

Furthermore, the presence of a fourth-order derivative in the Taylor expansion is consistent with expectations from r-mode theory, which enables braking indices analysis with a separated r-mode contribution term, quantifying the r-mode contribution. Our model accurately captures spin-down trends and complements glitch-based corrections to the rotational history. Without including the fourth-order

PSR	n (Est.)	n (Obs.)	n % Error	m (Est.)	m (Obs.)	m % Error
B0531+21 (Crab)	2.33	2.32	0.43%	45.33	45.33	0.00%
B1509-58	2.83	2.84	0.35%	13.53	14.5	6.69%
J1023-5746	66.71	66.8	0.13%	297314.50	298000	0.23%
J1418-6058	29.96	30.02	0.20%	2436392.81	2460000	0.96%

Table 4: Comparison of estimated and observed braking indices n and m for selected pulsars from the ATNF database. Observed values are derived from timing measurements of frequency derivatives. Model predictions use Eq. (40) and (41) with parameters in Table 5. Deviations may reflect unmodeled glitches or internal dynamics (68).

PSR	Crab	J1023-5746	J1418-6058	B2234+61
f (Hz)	29.947	8.971	9.044	2.019
s (Hz)	1.28×10^{-10}	2.97×10^{-6}	5.37×10^{-6}	2.58×10^{-6}
r (Hz $^{-1}$)	-3.43×10^{-13}	-1.09×10^{-7}	-1.91×10^{-7}	-1.87×10^{-6}
g (Hz $^{-3}$)	3.22×10^{-16}	1.34×10^{-9}	2.27×10^{-9}	4.49×10^{-7}
l (Hz $^{-5}$)	-9.36×10^{-20}	-5.46×10^{-12}	-8.96×10^{-12}	-3.60×10^{-8}

Table 5: Spin-down parameters for four selected pulsars from the Australia Telescope National Facility Pulsar Database (69).

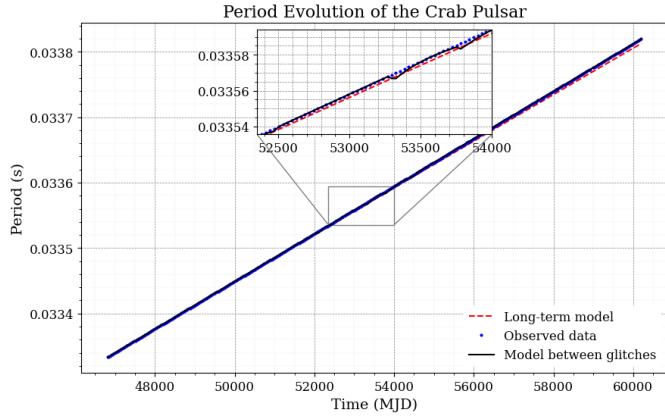


Figure 5: Pulsar period evolution for PSR B0531+21. The zoom-in between MJD 52350 and 54000 highlights spin-down discontinuities caused by glitches.

term, the Chishti et al. 2018 (64) model produces an average relative error of 2.88% using Crab pulsar data, while the inclusion of the fourth-order term produces an average relative error of 0.01% using the same set of Crab pulsar data and the fitting algorithm.

6. Discussion

Continuous gravitational waves (CWs) in narrow frequency bands are prime targets for next-generation detectors, particularly from rotating neutron stars and binary compact objects. Neutron stars with deformations or “mountains” are anticipated sources of persistent emission, offering unique insight into interior structure, equation of

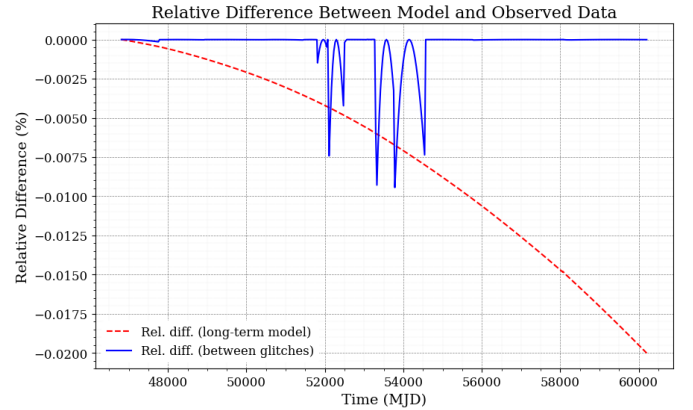


Figure 6: Relative difference between data and model fits. The long-term fit shows systematic drift, while between-glitch fits reveal localized jumps near glitch epochs.

Glitch Range (MJD)	t_0 (MJD)	f_0 (Hz)	f'_0 (Hz/s)	f''_0 (Hz/s ²)	f'''_0 (Hz/s ³)	f''''_0 (Hz/s ⁴)
46812 - 47767.4	47084	29.99	-3.786×10^{-10}	2.367×10^{-21}	-1.23×10^{-24}	4.567×10^{-24}
... [Remaining rows unchanged for brevity] ... 58065 - 60202	59138	29.6	-3.68×10^{-10}	1.169×10^{-20}	-3.415×10^{-24}	1.13×10^{-23}

Table 6: Frequency and its derivatives for selected glitch ranges, estimated using Eq. (42). Missing values (e.g., MJD 52083.8–52146 and MJD 53254.2–53331.1) are due to incomplete observational coverage (71).

state (EoS), and transport properties (72). Despite the absence of direct CW detections to date, searches—especially for r-mode-driven signals—are maturing rapidly in both sensitivity and technique.

Previous studies have investigated saturation amplitudes of r-modes under realistic astrophysical conditions and found them to be extremely small (36). Advanced data analysis methods (73; 74) and upgrades to gravitational wave observatories (75; 76; 77; 78; 50) continue to improve detection prospects.

Notably, targeted CW searches for specific pulsars—such as PSR J0537–6910—have placed upper limits on both frequency and amplitude for r-mode gravitational wave emission (14). If an r-mode signal is independently detected, our expressions in Eqs. (19) and (23) can be used to infer neutron star compactness and tidal deformability in an equation-of-state-independent manner.

Additionally, (16) have shown that observed spin-down in the Crab pulsar and others places stringent empirical constraints on r-mode amplitudes, typically $\alpha \lesssim 10^{-4}$. These findings support the physical plausibility of our low-amplitude r-mode models and further motivate the search for continuous gravitational waves from young pulsars within the sensitivity range of advanced detectors.

This work also contributes to improving timing residual analysis and enhancing sensitivity to CW signals in Pulsar Timing Arrays (PTAs). By linking time-dependent r-mode amplitude and rotational frequency to observable timing behavior, our model supports future CW detection strategies. This approach aligns with earlier results from (79), who showed how angular momentum exchange during thermonuclear bursts induces significant timing fluctuations.

We also emphasize that our model connects the r-mode gravitational wave frequency and amplitude with traditional timing observables, such as braking indices and period evolution. These r-mode-dependent expressions allow time-resolved estimates of gravitational wave strain, with direct application to real-time pulsar monitoring.

Our analytical expressions for compactness, tidal deformability, and r-mode frequency are equation-of-state independent and can be directly substituted into time-dependent spin-down and period models. This makes the method ideal for young or accreting pulsars in the non-linear saturation regime, where r-modes contribute a dominant seventh-order spin-down term (39). While magnetic dipole emission remains the largest spin-down torque in most scenarios, our results show that even small-amplitude r-modes affect braking indices, timing residuals, and fre-

quency evolution in measurable ways. The flexibility of our formalism allows negative spin-down coefficients, accommodating phenomena such as glitches and post-glitch recovery.

In the case of the Crab pulsar, our glitch modeling reveals a cumulative exponential slowdown effect. We find that long-term fits underestimate the period during glitch epochs, while piecewise fits between glitches better reproduce the observed behavior. This motivates more advanced theoretical models of glitch-triggered r-mode activation, which may also influence gravitational wave emission.

Future work will extend our model to glitch-prone pulsars like PSR J0537–6910 (80), exploring the possibility of using timing irregularities as indicators of r-mode activity. While the use of higher-order frequency derivatives carries a risk of overfitting, the demonstrated success of our approach on the Crab pulsar suggests this tradeoff is worthwhile in data-rich cases.

Finally, our analytic framework enables integration with search pipelines for continuous gravitational waves, including statistical techniques like F/G statistics and $5n$ -vector models (14). By expressing pulsar timing dynamics in terms of high-order frequency derivatives and r-mode amplitudes, we provide a compact and efficient toolset for modeling spin evolution, improving phase tracking, and refining CW detection.

7. Conclusions

In this study, we explored pulsar spin-down dynamics with an emphasis on the contribution of r-mode instabilities, particularly in the context of gravitational wave (GW) emission and neutron star structure. We formulated and solved a non-linear differential equation that incorporates r-mode losses, leading to time-dependent solutions for the rotational frequency and pulsar period. These solutions were validated against high-precision observational data from the Crab pulsar, exhibiting strong agreement and confirming the utility of the model.

We introduced Lambert W-based analytical solutions for neutron star compactness and tidal deformability as functions of r-mode gravitational wave frequency. These formulations are independent of the equation of state (EoS), allowing robust parameter estimation across a wide class of neutron star models. In particular, the application of Lambert-Tsallis functions enables the inversion of non-linear relations between r-mode frequency and physical parameters, further enriching the model’s predictive

capability.

The model’s capacity to yield seventh-order spin-down terms from r-mode effects demonstrates its relevance for understanding neutron stars in non-linear saturation regimes. While magnetic dipole radiation remains the dominant spin-down mechanism in most scenarios, accurate modeling of r-mode contributions enhances timing residual analyses, glitch modeling, and continuous gravitational wave signal interpretation. Our results support the inclusion of r-mode terms in practical GW search algorithms, particularly those targeting young and rapidly rotating neutron stars.

With the development of third-generation gravitational wave detectors such as the Einstein Telescope and Cosmic Explorer, r-mode signals—previously inaccessible—may soon become detectable. We share the optimism of Armas et al. (36) that r-mode GW emissions from nascent neutron stars and low-mass X-ray binaries could be within reach of enhanced detector sensitivities. In the long term, the interplay of r-modes with neutron star oscillations, glitches, and EoS-dependent properties could reveal deeper layers of stellar microphysics.

In conclusion, this work contributes to a consistent analytical and numerical framework for connecting r-mode physics to pulsar observations and gravitational wave signals. Our model serves as a foundation for further research into spin-down evolution, multi-messenger astrophysics, and the characterization of neutron star interiors.

Acknowledgements

The authors express their sincere gratitude to R. V. Ramos and K. Z. Nobrega at the Universidade Federal do Ceará for their invaluable support in the numerical evaluation of our Lambert-Tsallis solutions and for productive discussions that greatly contributed to this work. We also thank Reed Essick and Cecilia Chirenti for their insightful and informative input, which helped refine our theoretical approach.

We thank the anonymous reviewers for their inspiring and thorough critique of our manuscript.

This research was supported by the Mathematics of Information Technology and Complex Systems (MITACS) Globalink program, which provided the platform and funding for this collaborative effort. We are grateful to MITACS Globalink for their commitment to fostering research and international academic partnerships.

References

- [1] D. R. Lorimer, M. Kramer, *Handbook of Pulsar Astronomy*, Vol. 4, 2004.
- [2] J. H. Taylor, D. R. Stinebring, Recent progress in the understanding of pulsars., *araa* 24 (1986) 285–327. doi:10.1146/annurev.aa.24.090186.001441.
- [3] J. Taylor, Joseph H., Millisecond pulsars: nature’s most stable clocks., *IEEE Proceedings* 79 (1991) 1054–1062.

- [4] D. N. Matsakis, J. H. Taylor, T. M. Eubanks, A statistic for describing pulsar and clock stabilities., *aap* 326 (1997) 924–928.
- [5] J. Papaloizou, J. E. Pringle, Gravitational radiation and the stability of rotating stars., *Monthly Notices of the Royal Astronomical Society* 184 (1978) 501–508. doi:10.1093/mnras/184.3.501.
- [6] J. Provost, G. Berthomieu, A. Rocca, Low Frequency Oscillations of a Slowly Rotating Star - Quasi Toroidal Modes, *aap* 94 (1981) 126.
- [7] N. Andersson, K. D. Kokkotas, Towards gravitational wave asteroseismology, *Monthly Notices of the Royal Astronomical Society* 299 (4) (1998) 1059–1068. arXiv:gr-qc/9711088, doi:10.1046/j.1365-8711.1998.01840.x.
- [8] J. L. Friedman, S. M. Morsink, Axial Instability of Rotating Relativistic Stars, *The Astrophysical Journal* 502 (2) (1998) 714–720. arXiv:gr-qc/9706073, doi:10.1086/305920.
- [9] N. Andersson, A new class of unstable modes of rotating relativistic stars, *The Astrophysical Journal* 502 (2) (1998) 708–713. doi:10.1086/305919. URL <https://doi.org/10.1086/305919>
- [10] S. Abbassi, M. Reutord, V. Rezanian, An r-mode in a magnetic rotating spherical layer: application to neutron stars, *Monthly Notices of the Royal Astronomical Society* 419 (4) (2012) 2893–2899.
- [11] B. P. Abbott, R. Abbott, T. D. Abbott, et al., Gw150914: The advanced ligo detectors in the era of first discoveries, *Physical Review Letters* 116 (24) (2016) 241103. doi:10.1103/PhysRevLett.116.241103.
- [12] T. Akutsu, M. Ando, et al., Kagra: 2.5 generation interferometric gravitational wave detector, *Nature Astronomy* 3 (1) (2019) 35–40. doi:10.1038/s41550-018-0658-y. URL <http://dx.doi.org/10.1038/s41550-018-0658-y>
- [13] R. Abbott, T. Abbott, F. Acernese, et al., First search for nontensorial gravitational waves from known pulsars, *Phys. Rev. Lett.* 120 (2018) 031104. doi:10.1103/PhysRevLett.120.031104. URL <https://link.aps.org/doi/10.1103/PhysRevLett.120.031104>
- [14] R. Abbott, T. D. Abbott, S. Abraham, F. Acernese, L. S. Collaboration, Constraints from LIGO o3 data on gravitational-wave emission due to r-modes in the glitching pulsar PSR j0537–6910, *The Astrophysical Journal* 922 (1) (2021) 71. doi:10.3847/1538-4357/ac0d52. URL <https://doi.org/10.3847/2F1538-4357%2Fac0d52>
- [15] B. J. Owen, L. Lindblom, C. Cutler, B. F. Schutz, A. Vecchio, N. Andersson, Gravitational waves from hot young rapidly rotating neutron stars, *Physical Review D* 58 (8) (1998) 084020. arXiv:gr-qc/9804044, doi:10.1103/PhysRevD.58.084020.
- [16] T. E. Strohmayer, S. Mahmoodifar, Implications of the r-mode instability for accreting millisecond pulsars: Evidence for low amplitude oscillations, *The Astrophysical Journal* 767 (1) (2013) 45. doi:10.1088/0004-637X/767/1/45.
- [17] L. Bildsten, G. Ushomirsky, Viscous Boundary-Layer Damping of R-Modes in Neutron Stars, *The Astrophysical Journal* 529 (1) (2000) L33–L36. arXiv:astro-ph/9911155, doi:10.1086/312454.
- [18] N. Andersson, D. I. Jones, K. D. Kokkotas, Strange stars as persistent sources of gravitational waves, *Monthly Notices of the Royal Astronomical Society* 337 (4) (2002) 1224–1232. arXiv:astro-ph/0111582, doi:10.1046/j.1365-8711.2002.05837.x.
- [19] B. Haskell, N. Degenaar, W. C. G. Ho, Constraining the physics of the r-mode instability in neutron stars with X-ray and ultraviolet observations, *Monthly Notices of the Royal Astronomical Society* 424 (1) (2012) 93–103. arXiv:1201.2101, doi:10.1111/j.1365-2966.2012.21171.x.
- [20] V. Rezanian, r-Modes in the Ocean of a Magnetic Neutron Star, *The Astrophysical Journal* 574 (2) (2002) 899–907. arXiv:astro-ph/0202105, doi:10.1086/341115.
- [21] M. Branchesi, M. Maggiore, D. Alonso, C. Badger, et al., Science with the einstein telescope: a comparison of different designs (2023). arXiv:2303.15923.

- [22] M. Evans, R. X. Adhikari, C. Afle, et al., A horizon study for cosmic explorer: Science, observatories, and community (2021). [arXiv:2109.09882](https://arxiv.org/abs/2109.09882).
- [23] P. Amaro-Seoane, H. Audley, S. Babak, J. Baker, et al., Laser interferometer space antenna (2017). [arXiv:1702.00786](https://arxiv.org/abs/1702.00786).
- [24] W.-H. Ruan, Z.-K. Guo, R.-G. Cai, Y.-Z. Zhang, Taiji program: Gravitational-wave sources, *International Journal of Modern Physics A* 35 (17) (2020) 2050075. doi:10.1142/S0217751X2050075X.
- [25] J. Luo, L.-S. Chen, H.-Z. Duan, Y.-G. Gong, S. Hu, J. Ji, Q. Liu, J. Mei, V. Milyukov, M. Sazhin, Y.-Y. Shao, Z.-G. Silan, Z.-K. Hu, M.-E. Tobar, Y. Wang, H. Wang, Y. Xu, M. Yan, Y.-L. Zhang, Z.-B. Zhou, Tianqin: a space-borne gravitational wave detector, *Classical and Quantum Gravity* 33 (3) (2016) 035010. doi:10.1088/0264-9381/33/3/035010.
- [26] G. Agazie, A. Anumalapudi, A. M. Archibald, others, Nanograv Collaboration, The NANOGrav 15 yr Data Set: Evidence for a Gravitational-wave Background, *apjl* 951 (1) (2023) L8. [arXiv:2306.16213](https://arxiv.org/abs/2306.16213), doi:10.3847/2041-8213/acdac6.
- [27] R. N. Manchester, The international pulsar timing array, *Classical and Quantum Gravity* 30 (22) (2013) 224010. doi:10.1088/0264-9381/30/22/224010. URL <https://dx.doi.org/10.1088/0264-9381/30/22/224010>
- [28] G. Hobbs, A. Archibald, Z. Arzoumanian, D. Backer, et al., The international pulsar timing array project: using pulsars as a gravitational wave detector, *Classical and Quantum Gravity* 27 (8) (2010) 084013. doi:10.1088/0264-9381/27/8/084013. URL <https://dx.doi.org/10.1088/0264-9381/27/8/084013>
- [29] A. Weltman, P. Bull, S. Camera, K. Kelley, et al., Fundamental physics with the square kilometre array, *Publications of the Astronomical Society of Australia* 37 (2020). doi:10.1017/pasa.2019.42. URL <https://doi.org/10.1017/2Fpasa.2019.42>
- [30] S. Ghosh, D. Pathak, D. Chatterjee, Relativistic correction to the r-mode frequency in light of multimessenger constraints, *The Astrophysical Journal* 944 (1) (2023) 53. doi:10.3847/1538-4357/acb0d3. URL <https://doi.org/10.3847/2F1538-4357/2Facb0d3>
- [31] T. Gold, Rotating Neutron Stars as the Origin of the Pulsating Radio Sources, *Nature* 218 (5143) (1968) 731–732. doi:10.1038/218731a0.
- [32] F. Pacini, Rotating Neutron Stars, Pulsars and Supernova Remnants, *Nature* 219 (5150) (1968) 145–146. doi:10.1038/219145a0.
- [33] J. P. Ostriker, J. E. Gunn, On the Nature of Pulsars. I. Theory, *The Astrophysical Journal* 157 (1969) 1395. doi:10.1086/150160.
- [34] A. Ferrari, R. Ruffini, Theoretical Implications of the Second Time Derivative of the Period of the Pulsar NP 0532, *apjl* 158 (1969) L71. doi:10.1086/180435.
- [35] J. Papaloizou, J. E. Pringle, Non-radial oscillations of rotating stars and their relevance to the short-period oscillations of cataclysmic variables, *Monthly Notices of the Royal Astronomical Society* 182 (3) (1978) 423–442. [arXiv:https://academic.oup.com/mnras/article-pdf/182/3/423/3856018/mnras182-0423.pdf](https://academic.oup.com/mnras/article-pdf/182/3/423/3856018/mnras182-0423.pdf), doi:10.1093/mnras/182.3.423. URL <https://doi.org/10.1093/mnras/182.3.423>
- [36] P. Arras, E. E. Flanagan, S. M. Morsink, A. K. Schenk, S. A. Teukolsky, I. Wasserman, Saturation of the r-Mode Instability, *The Astrophysical Journal* 591 (2) (2003) 1129–1151. [arXiv:astro-ph/0202345](https://arxiv.org/abs/astro-ph/0202345), doi:10.1086/374657.
- [37] L. Lindblom, J. E. Tohline, M. Vallisneri, Nonlinear evolution of the r-modes in neutron stars, *Astrophysical Journal* 591 (2003) 1129–1151.
- [38] Alvarez, C., Carramiñana, A., Monopolar pulsar spin-down, *A&A* 414 (2) (2004) 651–658. doi:10.1051/0004-6361:20031627. URL <https://doi.org/10.1051/0004-6361:20031627>
- [39] L. Lindblom, B. J. Owen, S. M. Morsink, Gravitational radiation instability in hot young neutron stars, *Physical Review Letters* 80 (22) (1998) 4843–4846. doi:10.1103/physrevlett.80.4843. URL <https://doi.org/10.1103/2Fphysrevlett.80.4843>
- [40] N. Andersson, K. D. Kokkotas, N. Stergioulas, On the relevance of the r-mode instability for accreting neutron stars and white dwarfs, *The Astrophysical Journal* 516 (1) (1999) 307–314. doi:10.1086/307082. URL <https://doi.org/10.1086/2F307082>
- [41] N. K. Glendenning, S. Pei, F. Weber, Signal of quark deconfinement in the timing structure of pulsar spin-down, *Phys. Rev. Lett.* 79 (1997) 1603–1606. doi:10.1103/PhysRevLett.79.1603. URL <https://link.aps.org/doi/10.1103/PhysRevLett.79.1603>
- [42] M. G. Alford, K. Schwenzer, The instability and non-linear dynamics of rotating stars, *Monthly Notices of the Royal Astronomical Society* 437 (2) (2014) 1220–1235. doi:10.1093/mnras/stt1965.
- [43] P. Pani, L. Gualtieri, V. Ferrari, Tidal love numbers of a slowly spinning neutron star, *Phys. Rev. D* 92 (2015) 124003. doi:10.1103/PhysRevD.92.124003. URL <https://link.aps.org/doi/10.1103/PhysRevD.92.124003>
- [44] A. Mastrano, P. D. Lasky, A. Melatos, Neutron star deformation due to multipolar magnetic fields, *Monthly Notices of the Royal Astronomical Society* 434 (2) (2013) 1658–1667. doi:10.1093/mnras/stt1131.
- [45] S. Chandrasekhar, Solutions of Two Problems in the Theory of Gravitational Radiation, *Physical Review Letters* 24 (11) (1970) 611–615. doi:10.1103/PhysRevLett.24.611.
- [46] J. L. Friedman, B. F. Schutz, Lagrangian perturbation theory of nonrelativistic fluids., *The Astrophysical Journal* 221 (1978) 937–957. doi:10.1086/156098.
- [47] L. Lindblom, J. E. Tohline, M. Vallisneri, Nonlinear evolution of the r-modes in neutron stars, *Physical Review Letters* 86 (7) (2001) 1152–1155. doi:10.1103/physrevlett.86.1152. URL <https://doi.org/10.1103/physrevlett.86.1152>
- [48] A. Idrisy, B. J. Owen, D. I. Jones, R -mode frequencies of slowly rotating relativistic neutron stars with realistic equations of state, *Physical Review D* 91 (2) (jan 2015). doi:10.1103/physrevd.91.024001. URL <https://doi.org/10.1103/2Fphysrevd.91.024001>
- [49] R. Abbott, T. Abbott, S. Abraham, et al., Constraints from LIGO o3 data on gravitational-wave emission due to r-modes in the glitching pulsar PSR j0537–6910, *The Astrophysical Journal* 922 (1) (2021) 71. doi:10.3847/1538-4357/ac0d52. URL <https://doi.org/10.3847/2F1538-4357/2Fac0d52>
- [50] R. Abbott, et al., All-sky search for continuous gravitational waves from isolated neutron stars in the early third observing run of advanced ligo and advanced virgo, *Physical Review D* 104 (2021) 082004. doi:10.1103/PhysRevD.104.082004.
- [51] N. Andersson, Gravitational waves from instabilities in relativistic stars, *Classical and Quantum Gravity* 20 (7) (2003) R105–R144. doi:10.1088/0264-9381/20/7/201. URL <https://doi.org/10.1088/0264-9381/20/7/201>
- [52] K. H. Lockitch, J. L. Friedman, Where are the r-modes of isentropic stars?, *The Astrophysical Journal* 521 (2) (1999) 764–788. doi:10.1086/307580. URL <https://doi.org/10.1086/2F307580>
- [53] S. Yoshida, U. Lee, Rotational modes of nonisentropic stars and the gravitational radiation-driven instability, *The Astrophysical Journal Supplement Series* 129 (1) (2000) 353–366. doi:10.1086/313410. URL <https://doi.org/10.1086/2F313410>
- [54] S. Yoshida, S. Yoshida, Y. Eriguchi, R-mode oscillations of rapidly rotating barotropic stars in general relativity: analysis by the relativistic Cowling approximation, *Monthly Notices of the Royal Astronomical Society* 356 (1) (2005) 217–224. [arXiv:https://academic.oup.com/mnras/article-pdf/356/1/217/3586617/356-1-217.pdf](https://academic.oup.com/mnras/article-pdf/356/1/217/3586617/356-1-217.pdf), doi:10.1111/j.1365-2966.2004.08436.x. URL <https://doi.org/10.1111/j.1365-2966.2004.08436.x>

- [55] S. Caride, R. Inta, B. J. Owen, B. Rajbhandari, How to search for gravitational waves from r -modes of known pulsars, *Phys. Rev. D* 100 (2019) 064013. doi:10.1103/PhysRevD.100.064013. URL <https://link.aps.org/doi/10.1103/PhysRevD.100.064013>
- [56] Y. Levin, G. Ushomirsky, Crust-core coupling and r -mode damping in neutron stars: a toy model, *mnras* 324 (4) (2001) 917–922. arXiv:astro-ph/0006028, doi:10.1046/j.1365-8711.2001.04323.x.
- [57] F. E. Marshall, E. V. Gotthelf, W. Zhang, J. Middleditch, Q. D. Wang, Discovery of an Ultrafast X-Ray Pulsar in the Supernova Remnant N157B, *apjl* 499 (2) (1998) L179–L182. arXiv:astro-ph/9803214, doi:10.1086/311381.
- [58] R. Corless, G. Gonnet, D. Hare, D. Jeffrey, D. Knuth, On the lambert w function, *Advances in Computational Mathematics* 5 (1996) 329–359. doi:10.1007/BF02124750.
- [59] É. É. Flanagan, T. Hinderer, Constraining neutron-star tidal love numbers with gravitational-wave detectors, *Physical Review D* 77 (2) (jan 2008). doi:10.1103/physrevd.77.021502. URL <https://doi.org/10.1103/PhysRevD.77.021502>
- [60] T. Hinderer, Tidal love numbers of neutron stars, *The Astrophysical Journal* 677 (2) (2008) 1216–1220. doi:10.1086/533487. URL <https://doi.org/10.1086/533487>
- [61] P. K. Gupta, A. Puecher, P. T. H. Pang, J. Janquart, G. Koekoek, C. V. D. Broeck, Determining the equation of state of neutron stars with einstein telescope using tidal effects and r -mode excitations from a population of binary inspirals (2022). arXiv:2205.01182.
- [62] LIGO Scientific Collaboration, LALSuite: LIGO Scientific Collaboration Algorithm Library Suite, *Astrophysics Source Code Library*, record ascl:2012.021 (Dec. 2020). arXiv:2012.021.
- [63] B. J. Owen, L. Lindblom, C. Cutler, B. F. Schutz, A. Vecchio, N. Andersson, Gravitational waves from hot young rapidly rotating neutron stars, *Phys. Rev. D* 58 (1998) 084020. doi:10.1103/PhysRevD.58.084020. URL <https://link.aps.org/doi/10.1103/PhysRevD.58.084020>
- [64] F. A. Chishtie, X. Zhang, S. R. Valluri, An analytic approach for the study of pulsar spindown, *Classical and Quantum Gravity* 35 (14) (2018) 145012. doi:10.1088/1361-6382/aac9d6. URL <https://dx.doi.org/10.1088/1361-6382/aac9d6>
- [65] A. G. Lyne, R. S. Pritchard, F. G. Smith, Crab Pulsar timing 1982–87, *Monthly Notices of the Royal Astronomical Society* 233 (3) (1988) 667–676. arXiv:https://academic.oup.com/mnras/article-pdf/233/3/667/3136003/mnras233-0667.pdf, doi:10.1093/mnras/233.3.667. URL <https://doi.org/10.1093/mnras/233.3.667>
- [66] R. N. Manchester, J. M. Durdin, L. M. Newton, A second measurement of a pulsar braking index, *Nature* 313 (6001) (1985) 374–376. doi:10.1038/313374a0.
- [67] R. Bondarescu, S. A. Teukolsky, I. Wasserman, Spinning down newborn neutron stars: Nonlinear development of the r -mode instability, *Physical Review D* 76 (2007) 064019. doi:10.1103/PhysRevD.76.064019.
- [68] C. M. Espinoza, Braking indices and spin evolution: something is loose inside neutron stars, *Proceedings of the International Astronomical Union* 13 (S337) (2017) 221–224. doi:10.1017/S1743921317008535. URL <https://doi.org/10.1017/S1743921317008535>
- [69] R. N. Manchester, G. B. Hobbs, A. Teoh, M. Hobbs, The australia telescope national facility pulsar catalogue, *The Astronomical Journal* 129 (4) (2005) 1993–2006. doi:10.1086/428488. URL <https://doi.org/10.1086/428488>
- [70] A. G. Lyne, R. S. Pritchard, F. Graham Smith, 23 years of Crab pulsar rotational history., *mnras* 265 (1993) 1003–1012. doi:10.1093/mnras/265.4.1003.
- [71] A. G. Lyne, C. A. Jordan, F. Graham-Smith, C. M. Espinoza, B. W. Stappers, P. Weltevrede, 45 years of rotation of the Crab pulsar, *Monthly Notices of the Royal Astronomical Society* 446 (1) (2014) 857–864. arXiv:https://academic.oup.com/mnras/article-pdf/446/1/857/4154426/stu2118.pdf, doi:10.1093/mnras/stu2118. URL <https://doi.org/10.1093/mnras/stu2118>
- [72] N. Lu, K. Wette, S. M. Scott, A. Melatos, Inferring neutron star properties with continuous gravitational waves, *mnras* 521 (2) (2023) 2103–2113. arXiv:2209.10981, doi:10.1093/mnras/stad390.
- [73] R. Tenorio, D. Keitel, A. M. Sintes, Search methods for continuous gravitational-wave signals from unknown sources in the advanced-detector era, *Universe* 7 (12) (2021) 474. doi:10.3390/universe7120474. URL <http://dx.doi.org/10.3390/universe7120474>
- [74] P. Jaranowski, A. Królak, B. F. Schutz, Data analysis of gravitational-wave signals from spinning neutron stars: The signal and its detection, *Phys. Rev. D* 58 (1998) 063001. doi:10.1103/PhysRevD.58.063001. URL <https://link.aps.org/doi/10.1103/PhysRevD.58.063001>
- [75] B. P. Abbott, R. Abbott, T. D. Abbott, et al., Gw170817: Observation of gravitational waves from a binary neutron star inspiral, *Phys. Rev. Lett.* 119 (2017) 161101. doi:10.1103/PhysRevLett.119.161101. URL <https://link.aps.org/doi/10.1103/PhysRevLett.119.161101>
- [76] M. Pitkin, C. Gill, D. I. Jones, G. Woan, G. S. Davies, First results and future prospects for dual-harmonic searches for gravitational waves from spinning neutron stars, *Monthly Notices of the Royal Astronomical Society* 453 (4) (2015) 4399–4420. arXiv:https://academic.oup.com/mnras/article-pdf/453/4/4399/8035169/stv1931.pdf, doi:10.1093/mnras/stv1931. URL <https://doi.org/10.1093/mnras/stv1931>
- [77] R. Abbott, et al., Search for continuous gravitational waves from young neutron stars in the first half of advanced ligo and virgo’s third observing run, *Physical Review D* 105 (2) (2022) 022002. doi:10.1103/PhysRevD.105.022002.
- [78] R. Abbott, et al., All-sky search for continuous gravitational waves from isolated neutron stars in o3a with advanced ligo and virgo, *Physical Review D* 105 (8) (2022) 082005. doi:10.1103/PhysRevD.105.082005.
- [79] V. Rezanian, Large frequency drifts during type i x-ray bursts, arXiv preprint astro-ph/0304153v2 (2003).
- [80] W. C. G. Ho, C. M. Espinoza, et al., Return of the big glitcher: Nicer timing and glitches of psr j0537-6910, *Monthly Notices of the Royal Astronomical Society* 498 (4) (2020) 4605–4614. arXiv:https://academic.oup.com/mnras/article-pdf/498/4/4605/33798603/staa2640.pdf, doi:10.1093/mnras/staa2640. URL <https://doi.org/10.1093/mnras/staa2640>
- [81] S. R. Valluri, D. J. Jeffrey, R. M. Corless, Some applications of the lambert w function to physics, *Canadian Journal of Physics* 78 (9) (2000) 823–831. arXiv:https://doi.org/10.1139/p00-065, doi:10.1139/p00-065. URL <https://doi.org/10.1139/p00-065>
- [82] G. da Silva, R. Ramos, The lambert–tsallis w_q function, *Physica A: Statistical Mechanics and its Applications* 525 (2019) 164–170. doi:https://doi.org/10.1016/j.physa.2019.03.046. URL <https://www.sciencedirect.com/science/article/pii/S0378437119302791>
- [83] R. V. Ramos, Solving the fermat and fibonacci equations with the lambert-tsallis w_q function (2023). arXiv:2304.14140.

Appendix A. The Lambert W and Lambert-Tsallis Functions

The transcendental equation $z = W \exp W$ appeared in the mid-eighteenth century in Johann Heinrich Lambert’s investigations of logarithms and continued fractions. The

function was rediscovered by M. Wright in the context of branching processes, but it was not until the seminal paper of Corless et al. in 1996 (58) that the systematic branch structure were popularised. This work triggered a rapid expansion of applications across physics (81), chemistry, computer science, and combinatorics.

The classical Lambert W function is the multivalued inverse of the map $w \rightarrow we^w$. It is defined implicitly by

$$W(z)e^{W(z)} = z, \quad z \in \mathbb{C}. \quad (\text{A.1})$$

It possesses two real branches on $[-e^{-1}, 0)$, the principal branch W_0 and the lower branch W_{-1} , and an infinite set of complex branches.

The two useful identities frequently used are

$$\frac{dW}{dz} = \frac{W(z)}{z[1+W(z)]}, \quad W(ze^z) = z. \quad (\text{A.2})$$

Da Silva and Ramos generalized the Lambert function by replacing the usual exponential with the Tsallis q -exponential:

$$\exp_q(x) = [1 + (1-q)x]^{1/(1-q)}, \quad \exp_1(x) = e^x. \quad (\text{A.3})$$

in 2019 (82). The Lambert-Tsallis function is defined as

$$W_q(z)e_q^{W_q(z)} = z, \quad z \in \mathbb{C}. \quad (\text{A.4})$$

The solutions using the Lambert-Tsallis function were given to the fractional polynomials of the type $ax^\alpha + bx^\beta + c = 0$ (83):

$$x_1 = \left[\frac{a}{b} \left(\frac{\alpha}{\beta - \alpha} \right) W_{1 - \frac{\alpha}{\beta - \alpha}} \left(\frac{b}{a} \left(\frac{\beta - \alpha}{\alpha} \right) \left(-\frac{c}{a} \right)^{\frac{\beta - \alpha}{\alpha}} \right) \right]^{\frac{1}{\beta - \alpha}}, \quad (\text{A.5})$$

and

$$x_2 = \left[\frac{b}{a} \left(\frac{\beta}{\alpha - \beta} \right) W_{1 - \frac{\beta}{\alpha - \beta}} \left(\frac{a}{b} \left(\frac{\alpha - \beta}{\beta} \right) \left(-\frac{c}{b} \right)^{\frac{\alpha - \beta}{\beta}} \right) \right]^{\frac{1}{\alpha - \beta}}. \quad (\text{A.6})$$

Appendix B. Frequency Cubic Roots with Time-independent Coefficients

For the case where the spin-down coefficients $\{s, r, g, l\}$ are assumed to be constant, the general spin-down equation (7) becomes:

$$-dt = \frac{1}{\nu} \frac{d\nu}{s + r\nu^2 + g\nu^4 + l\nu^6}. \quad (\text{B.1})$$

By substituting $\nu^2 = x$ and thus $d\nu = \frac{dx}{2\sqrt{x}}$, this reduces to a rational integral involving a cubic denominator:

$$\frac{1}{2lx} \frac{dx}{(x-a)(x-b)(x-c)} = -dt, \quad (\text{B.2})$$

where $\{a, b, c\}$ are the **roots of the cubic polynomial** $lx^3 + gx^2 + rx + s$, which can be solved either analytically or numerically.

The general formula for the roots of a cubic polynomial is:

$$\begin{aligned} \{x_i\} &= -\frac{1}{3} \left(\frac{r}{s} + \epsilon^i C + \frac{\Delta_0}{\epsilon^i C} \right), \quad i = 0, 1, 2, \\ \text{where } \epsilon &= \frac{-1 + i\sqrt{3}}{2}, \\ C &= \sqrt[3]{\frac{\Delta_1 \pm \sqrt{\Delta_1^2 - 4\Delta_0^3}}{2}}, \\ \Delta_0 &= \left(\frac{g}{l} \right)^2 - 3\frac{r}{l}, \\ \Delta_1 &= 2 \left(\frac{g}{l} \right)^3 - 9\frac{gr}{l^2} + 27\frac{s}{l}. \end{aligned} \quad (\text{B.3})$$

Alternatively, this can be expressed in terms of complex radicals as:

$$\begin{aligned} \{a, b, c\} &= \left[A + \sqrt{A^2 + B^2} \right]^{1/3} + \left[A - \sqrt{A^2 + B^2} \right]^{1/3} - \frac{g}{3l}, \\ \text{where } A &= \frac{-g^3}{27l^3} + \frac{gr}{6l^2} - \frac{s}{2l}, \\ B &= \frac{r}{3l} - \frac{g^2}{9l^2}. \end{aligned} \quad (\text{B.4})$$

Appendix C. Period Analysis with Cubic Roots

As discussed in Appendix Appendix B, the roots $\{a, b, c\}$ represent the roots of the spin-down polynomial. Equation (31) can be integrated via partial fraction decomposition. Let P_0 and t_0 be the initial period and time. Then the integral becomes:

$$\begin{aligned} (b-a)c^2 \ln \left(\frac{K-c}{K_0-c} \right) + (a-c)b^2 \ln \left(\frac{K-b}{K_0-b} \right) + \\ (c-b)a^2 \ln \left(\frac{K-a}{K_0-a} \right) = -2s_0 t (b-a)(a-c)(c-b), \end{aligned} \quad (\text{C.1})$$

where $K = P^2$, $K_0 = P_0^2$, and we assume $t_c \gg t, t_0$ (64).

In practice, most root sets include one real root and a pair of complex conjugates: let $b = x + iy$, $c = x - iy$. Then Eq. (C.1) becomes:

$$\begin{aligned} [(x-a)(x^2-y^2) + 2xy^2] \left(\ln \frac{K-c}{K_0-c} - \ln \frac{K-b}{K_0-b} \right) \\ - 2iya^2 \ln \frac{K-a}{K_0-a} + i[y(x^2-y^2) - 2xy(x-a)] \times \\ \left(\ln \frac{K-c}{K_0-c} + \ln \frac{K-b}{K_0-b} \right) = -4iys_0 t (x^2 - 2ax + a^2 + y^2). \end{aligned} \quad (\text{C.2})$$

Using the identity $\ln z - \ln z^* = 2i \tan^{-1} \left(\frac{\text{Im}(z)}{\text{Re}(z)} \right)$ and simplifying the logarithmic terms, we recover the final implicit form for $P(t)$, given in Eq. (32).

Appendix D. Detailed Derivation of r-Mode Energy Loss

To ensure clarity and consistency, we outline here the derivation of r-mode energy loss due to gravitational radiation, following the frameworks of (63; 39). This derivation demonstrates how gravitational wave emission driven by current multipole radiation results in rotational energy loss in neutron stars.

The gravitational wave luminosity associated with r-mode oscillations is given by:

$$\dot{E}_{\text{r-mode}} = -\frac{32\pi^2\alpha^2 JMR^3\Omega^8}{c^7}, \quad (\text{D.1})$$

where α is the dimensionless r-mode amplitude, J is a structural constant dependent on the stellar model, M is the stellar mass, R is the radius, Ω is the angular velocity, and c is the speed of light.

This formula is derived by integrating the gravitational radiation power emitted from the current multipole $l = m = 2$ r-mode. The general gravitational wave energy loss rate for an r-mode is:

$$\dot{E}_{\text{GW}} = \frac{2}{3}\omega^6 |\tilde{J}|^2 \frac{R^7}{G}, \quad (\text{D.2})$$

where ω is the mode frequency in the rotating frame, and \tilde{J} is the current multipole moment scaling with the internal density distribution.

For the fundamental r-mode ($l = m = 2$), the frequency is related to the star's spin as:

$$\omega = \frac{2}{3}\Omega. \quad (\text{D.3})$$

Substituting this into Eq. (B2) yields:

$$\dot{E}_{\text{GW}} \propto \Omega^8, \quad (\text{D.4})$$

confirming that r-mode emission is strongly sensitive to the stellar spin rate.

The full derivation involves integrating the mode energy distribution and flux through a sphere enclosing the neutron star. The final coefficient depends on the structure of the mode and is encapsulated in the dimensionless integral:

$$J = \int_0^R \rho r^6 dr, \quad (\text{D.5})$$

where $\rho(r)$ is the stellar mass density profile.

Substituting this into the luminosity expression confirms the full form of r-mode energy loss:

$$\dot{E}_{\text{r-mode}} = -\frac{32\pi^2\alpha^2 JMR^3\Omega^8}{c^7}, \quad (\text{D.6})$$

This equation encapsulates the dominant frequency scaling and structural dependencies, and is consistent with numerical studies and analytical estimates from (63; 39).